Tellus (1999), 51A, 833–853
Printed in UK. All rights reserved

TELLUS
ISSN 0280–6495

Relation between the meridional distribution of potential vorticity and the Lagrangian mean circulation in the troposphere

By MASAKI SATOH, *Centre for Atmospheric Science, DAMTP, University of Cambridge, Silver Street, Cambridge, CB3 9EW, UK*

(Manuscript received 3 September 1998; in final form 18 May 1999)

ABSTRACT

The meridional distribution of potential vorticity (PV) in the troposphere is examined in terms of the Lagrangian transport by using an idealistic general circulation model. A zonally uniform forcing and uniform boundary conditions are applied to the model to particularly examine the PV structure in the mid-latitudes and the subtropics. Trajectories of air parcels released from each grid point of the model and Lagrangian changes in PV are calculated for a period of 60 days. Values of PV of each parcel are changing along the Lagrangian motions due to the diabatic effect, the frictional effect and the mixing effect which has smaller scales than those resolvable in the model. Both diabatic and frictional effects are dominant in the lower layers, and the mixing effect is larger in the other regions. It is found that the zonal mean PV changes have different characteristics between the "Underworld" in which isentropes intersect the ground and the "Middleworld" in which isentropes are above the ground and intersect the tropopause. In the Underworld, the zonal mean PV changes are determined by the equatorial flow in the lower layers. In particular, the PV changes are negative in the lower layers of the low- and the mid-latitudes. (The sign of PV tendency is for the northern hemisphere. The southern hemispheric tendency is opposite as in the followings.) This negative tendency is due to the diabatic effect near the surface. In the Middleworld, there remain positive and negative tendency regions, which are resulted from the isentropic mixing. In general, if a parcel moves poleward in the mid-latitudes, the value of PV increases, whereas the value of PV decreases if a parcel moves equatorward. The sign of the Lagrangian mean change in PV corresponds to whether the Lagrangian mean motions cross the PV contours equatorward or poleward in the meridional plane. In particular, the contour of no change in PV has a similar shape to that of meridional distribution of PV in the mid-latitudes. This indicates that the directions of the Lagrangian mean motions are very close to those of the isolines of PV at the points on this contour.

1. Introduction

The meridional distributions of potential temperature and potential vorticity (hereafter, PV) reflect many of the key rôles in the dynamics of climate states of the atmosphere (Hoskins, 1991; Sun and Lindzen, 1994). Since both potential temperature and PV are conservative quantities under adiabatic and frictionless conditions, PV analysis on isentropic surfaces is an important tool for predictions of extratropic synoptic scale disturbances (Hoskins et al., 1985). However, although these two quantities are conservative for the time scale of synoptic eddies, i.e., a week or so, their changes cannot be negligible for a longer

* Corresponding address: Masaki Satoh, Saitama Insitute of Technology, 1690 Fusaiji, Okabe, Oosato, Saitama, 369-0293, Japan.
E-mail: satoh@sit.ac.jp.

time scale, say a month or several months, which is the time scale of the meridional circulation. Their changes together with the circulation of this time scale determine the meridional distributions of potential temperature and PV.

As for the potential temperature, the relation between its meridional distribution, its tendency and the meridional circulation is well understood. The vertical structure of potential temperature is close to the moist adiabat in the tropics due to the latent heat release of moist convection (Satoh, 1994), whereas it is conditionally unstable in the extratropics due to the baroclinic eddy statistics. As a result, isentropic surfaces are horizontal in the tropics and are inclined towards upper altitudes as latitudes become higher. The tendency of potential temperature, that is, the diabatic term, is positive in the deep tropics due to the latent heat release and in the boundary layers equatorward from the mid-latitudes due to the sensible heat flux from the surface. On the other hand, it is negative almost all over the extratropic troposphere due to the radiative cooling, except for the middle layers in the mid-latitudes where the latent heat release is associated with baroclinic eddies (Peixoto and Oort, 1992).

The meridional circulation can be obtained from the meridional distributions of potential temperature and its tendency. Here, it is the Lagrangian motion along each air parcel that is directly related to the Lagrangian change in potential temperature of the air parcel. The meridional circulation given by the zonal average of Lagrangian motions of air parcels is referred to the Lagrangian mean circulation (Andrews and McIntyre, 1978). The residual circulation, which is relatively easily calculated, is different from the Lagrangian mean circulation (Edmon et al., 1980; Andrews et al., 1987). The residual circulation, however, has a characteristic of the diabatic circulation which is a circulation driven by diabatic effects, and helps understandings of material transports in the meridional plane (Holton, 1992). It is also suggested that the residual circulation has a close resemblance to the zonal mean circulation averaged in the isentropic coordinates (McIntosh and McDougall, 1996; Karoly et al., 1997). One of the differences of the two circulations is that the isentropic mean circulation gives the equatorward flow in the lower layers, whereas the residual circulation does not resolve it (Townsend and Johnson, 1985; Johnson, 1989).

The streamlines of the residual circulation intersect the isentropic contours only where the diabatic effect exists. For instance, in the extratropic troposphere except for the lower layers of baroclinic zones, the streamlines of the residual circulation intersect the isentropes downgradient, since the diabatic terms are negative in this region. As a result, the residual circulation has a single cellar structure over the hemisphere like an extended Hadley cell toward the polar region (Edmon et al., 1980; Karoly et al., 1997). The Lagrangian mean circulation in the troposphere is also well known (Kida, 1983; Noda, 1988). There are similar structures between the Lagrangian mean circulation and the residual circulation: the cross-isentropic hemispheric scale circulation seen in the residual circulation also appears in the Lagrangian mean circulation. In the isentropic direction, however, there is a distinctive difference between the two circulations: the streamlines of the residual circulation are directed toward upper altitudes as latitudes become higher, whereas the Lagrangian mean circulation is convergent along the isentropic contours in the mid-latitudes (Noda, 1988). The divergent component does not exist in the residual circulation, whereas it generally exists in the Lagrangian mean circulation (Plumb, 1979; Plumb and Mahlman, 1987).

As for PV, there are also well known characteristics in the meridional distribution: a large difference between the troposphere and the stratosphere and a monotonicity in the latitudinal direction. The contours of PV are almost vertical in the low-latitudes, and their intervals become wider in the mid-latitudes of the troposphere as shown by Sun and Lindzen (1994, Fig. 2). Sun and Lindzen (1994) have presented an extreme view that PV is constant along isentropic surfaces in the extratropics and have tried to obtain the meridional distributions of potential temperature and zonal velocity.

In general, PV is not conservative if diabatic or frictional process exists (Haynes and McIntyre, 1987). In the free atmosphere above the surface boundary layers, the diabatic process is the main factor for the change in PV (Hoskins et al., 1985; Edouard et al., 1997). However, in the region of prevailing microstructure associated with development of extratropical cyclones, PV is thought to be homogenised by stirring and mixing process (McIntyre and Palmer, 1984; Pierrehumbert and Yang, 1993; Ambaum, 1997). A constant PV distribution along isentropes assumed by Sun and Lindzen (1994) should be ascribed to the mixing process along the isentropic surfaces.

In the Lagrangian circulation of the troposphere, both isentropic mixing motions and cross-isentropic flows exist (Kida, 1977; Noda, 1988). If air parcels are traced for more than a week, PV values of parcels will generally change due to the isentropic mixing and the diabatic process: PV will be homogenised by the isentropic mixing and will change its value along cross-isentropic flows if there is a vertical gradient in the tendency of potential temperature (Hoskins et al., 1985; Hoskins, 1991). It should be noted here that the impermeability theorem (Haynes and McIntyre, 1987, 1990), which states that there is no PV flux across isentropic surfaces even if diabatic cross-isentropic flow exists, does not give any constraint on the PV distribution. For instance, in the case of a steady circulation, the impermeability theorem states that PV fluxes across the steady isentropic surfaces are zero and is nothing but consistent with the steady PV field.

It does not seem that any attempt has been presented as to how PV changes if both isentropic mixing and cross-isentropic flows exist. Although the global PV budgets are analysed (Hoskins, 1991; Hoerling, 1992; Brunet et al., 1995; Edouard et al., 1997), there is no idea what is the relation between the meridional distribution of PV, its tendency and the meridional circulation. To establish such a relation, we need to know how the Lagrangian changes in PV is distributed in the meridional plane. From the comparison between the changes in PV and the meridional circulation in the Lagrangian sense, one could conjecture what are the important dynamical processes for specification of the meridional distribution of PV.

In the present study, relation between the Lagrangian changes in PV and the meridional circulation is examined with particular emphasis on the subtropics and the mid-latitudes, since the Lagrangian mean circulation as well as the residual circulation has a distinctive structure in the subtropics: the streamlines of the residual circulation turn their directions from the downward motion of the Hadley circulation to the upward motion along the isentropic contours (Karoly et al., 1997). The change in the directions in the subtropics can also be seen in the Lagrangian mean circulation (Noda, 1988). The circulation system of this region is believed to be related to the dynamics of the subtropical jet, the concentration of PV gradient and the abrupt change of tropopause heights. For this purpose, in the present study, we start from a simple framework by using an idealistic general circulation model in expectation of a clear meridional structure of PV in the subtropics.

The structure of the paper is as follows. In Section 2, an experimental design and a general circulation model used in this study are described with some statistic properties of the model results. The calculation procedure for trajectories of air parcels is also described. In Section 3, Lagrangian changes in PV values are obtained with the trajectory calculation, and the meridional distribution of PV change is compared with the Lagrangian mean circulation. Finally, relation between the meridional distribution of PV and the Lagrangian mean circulation are discussed in Section 4. A limitation of this study and further problems are also pointed out.

2. Model and trajectory calculation

In the present study, we use an idealistic general circulation model (GCM) in which a clear meridional structure of PV is produced in the subtropics. The model atmosphere contains a zonally uniform Hadley circulation in the low-latitudes and baroclinic unstable disturbances generated under a zonally uniform forcing in the extratropics. Results from the idealistic model help us in understanding complicated and ambiguous structures which might be seen in the real atmosphere. For example, in the PV budget analysis by Hoskins (1991), the characteristic dipole structure seen in the southern hemisphere is not clearly shown in the northern hemisphere. The zonally asymmetry of the circulation in the northern hemisphere might have diluted the dipole structure. Nevertheless, we should be careful to interpret model results since artificial assumptions might be introduced in the model and the statistics of the model outputs are not always relatable to the real atmosphere. This kind of caveat will be presented in Section 4.

The present GCM is based on Numaguti (1993) but physical processes are simplified as in the dynamical core experiment described in Held and Suarez (1994). The model is governed by the primitive equations with the σ-coordinates in the vertical: the resolution of the model is T42 with 48 levels, where $\sigma = p/p_s$, p is pressure and p_s is surface pressure. Locations of the vertical levels are described in Section 6.

The model atmosphere is dry without hydrologic cycle. No sensible and latent heat fluxes are allowed between the atmosphere and the surface. Diabatic heating is given by a Newtonian type radiation and an additional heating near the equator:

$$Q = \frac{T - T_{\mathrm{ref}}}{\tau_{\mathrm{R}}} + Q_{\mathrm{EQ}}, \tag{1}$$

where T_{ref} is a reference temperature of the Newtonian radiation, τ_{R} is a relaxation time, and Q_{EQ} is an additional heating which represents latent heat flux near the equator. T_{ref} has a smooth profile in the vertical direction, given by

$$T_{\mathrm{ref}}(\phi, z) = T_{\min} + [T_{\mathrm{rs}}(\phi) - T_{\min}] \times \left[1 - \tanh \frac{\Gamma z}{T_{\mathrm{rs}}(\phi) - T_{\min}}\right], \tag{2}$$

$$T_{\mathrm{rs}}(\phi) = T_{\mathrm{r0}} - \Delta T_{\mathrm{r}} \sin^2 \phi, \tag{3}$$

where ϕ is latitude, z is height, and Γ is the lapse rate of the reference temperature just above the surface. We use $T_{\mathrm{r0}} = 300\mathrm{K}$, $\Delta T_{\mathrm{r}} = 40$ K, $T_{\min} = 200$ K and a slightly stable stratification $\Gamma = 0.9$ K km^{-1}. Γ should be close to the neutral value, since the temperature profile is greatly dependent on the relaxation profile if a smaller Γ is given. The height z is calculated by the integration of the hydrostatic balance. As for the relaxation time τ_{R}, the same dependency proposed by Held and Suarez (1994) is used:

$$\tau_{\mathrm{R}}^{-1}(\phi, \sigma) = \begin{cases} \tau_{\mathrm{Ra}}^{-1} & \sigma < \sigma_{\mathrm{B}}, \\ \tau_{\mathrm{Ra}}^{-1} + (\tau_{\mathrm{Rs}}^{-1} - \tau_{\mathrm{Ra}}^{-1}) \dfrac{\sigma - \sigma_{\mathrm{B}}}{1 - \sigma_{\mathrm{B}}} \cos^4 \phi & \sigma \geqslant \sigma_{\mathrm{B}}, \end{cases} \tag{4}$$

where $\tau_{\mathrm{Ra}} = 40$ days, $\tau_{\mathrm{Rs}} = 4$ days, and $\sigma_{\mathrm{B}} = 0.8$. This shorter relaxation time represents the effect of sensible heat flux from the surface boundary. As pointed out by Held and Suarez (1994), if one gives a constant value for τ_{R} instead of the above formula, the stratification of the lower layers will be very stable. This is because the Newtonian radiation is not sufficient to heat up the cold equatorward flows in the lower layers. To obtain a realistic intensity of the Hadley circulation, an additional heating is given near the equatorial latitudes (Becker et al, 1997). This heating is given by

$$Q_{\mathrm{EQ}}(\phi, \sigma) = Q_0 \exp\left(-\frac{\phi^2}{\Delta\phi}\right) \sin\left(\pi \frac{\sigma_{\mathrm{B}} - \sigma}{\sigma_{\mathrm{B}} - \sigma_{\mathrm{T}}}\right), \tag{5}$$

where $\sigma_{\mathrm{B}} = 0.8$, $\sigma_{\mathrm{T}} = 0.2$, $\Delta\phi = 5°$, and $Q_0 = 3$ K day^{-1}. Effects of the momentum exchange between the surface and the atmosphere is represented by the Rayleigh friction following Held and Suarez (1994):

$$\boldsymbol{F}_{\mathrm{H}} = -\frac{\boldsymbol{v}_{\mathrm{H}}}{\tau_{\mathrm{F}}}, \tag{6}$$

where $\boldsymbol{v}_{\mathrm{H}}$ is horizontal winds and τ_{F} is a relaxation time. The relaxation coefficient (inverse of the relaxation time) for the Rayleigh friction is zero above the level $\sigma_{\mathrm{B}} = 0.8$, and linearly increases with σ below σ_{B}. The relaxation time just above the surface is $\tau_{\mathrm{F}} = 1$ day. In addition to the above formula, the numerical diffusion is introduced as a fourth power of Laplacian in vorticity, divergence and temperature fields. The decaying time for the most smallest horizontal scale is 1 day. The initial field of temperature is the same as T_{ref} except for a small perturbation and no motion is given initially. Integration is performed for 140 days. By the day 80 of the integration, the tropospheric circulation of the model can be regarded to be in a statistically equilibrium state.

Fig. 1 shows meridional distributions of the potential temperature, PV and the stream function of the residual circulation. Calculation method for PV is described in Section 5. The residual circulation is obtained according to Edmon et al. (1980). These fields are given by an average between the days 80 and 140. The overall structures of the potential temperature and PV are realistic as compared with those of the observational fields (e.g., Fig. 2 of Sun and Lindzen, 1994): a distinct PV difference between the troposphere and the stratosphere, abrupt change in the height of the PV-contours near the subtropic jets, and homogenised PV along isentropic surfaces in the mid-latitudes. In the lower levels, particularly in the high-latitudes, PV has relatively larger values

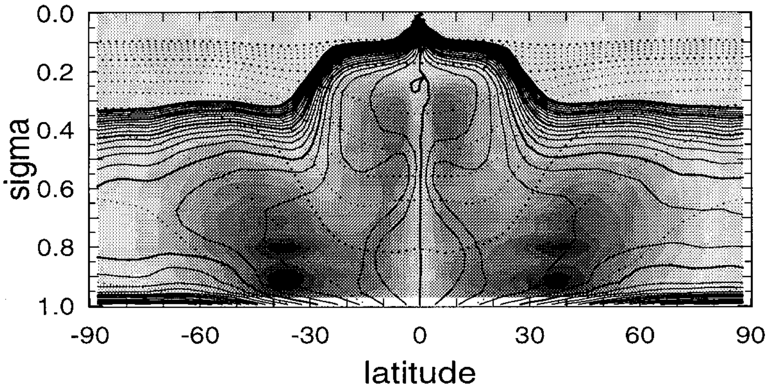

Fig. 1. Meridional distributions of zonally averaged PV, potential temperature and the residual circulation for the statistically equilibrium state of the model calculation. The solid lines show PV in the range from -2.0 PVU to $+2.0$ PVU with contour interval 0.1 PVU. The dotted lines show potential temperature from 270 K to 400K with contour interval 10 K. The gray scale shows the residual circulation. The thicker pattern means the larger values of the stream functions with a gradation of every 1×10^{10} kg/s.

because of insufficient heating by the Newtonian radiation (Held and Suarez, 1994). The other characteristic in the PV field of Fig. 1 is a tongue shape intruding the equatorial lower-PV zone in the middle level of the troposphere ($\sigma \approx 0.5$). This region seems to be connected with of the tropopause folding associated with the subtropic jets.

In addition to potential temperature and PV, Fig. 1 also shows the residual circulation. In each hemisphere, the residual circulation forms one cellar structure which consists of a direct circulation corresponding to the Hadley circulation in the low-latitudes and of upward inclined streamlines in the mid-latitudes. Except for the deep tropics and the boundary layers near the surface, the streamlines of the residual circulation cross the isentropes downgradient. In the real atmosphere, the streamlines are upgradient in the middle layers of the mid-latitudes (Edmon et al., 1980; Karoly et al, 1997), so that the result shown above has a somewhat different characteristic from the reality. This is because the diabatic heating due to latent heat release in the extratropics is not included in the model. The lack of moist effect in the extratropics may be justified if one reminds that baroclinic instability is understood in a framework of the dry atmosphere. To a first approximation for the argument of the global circulation, effects of latent heat release in the extratropics could be neglected. Therefore, we examine only the dry experiments in the present study. Possible effects of latent heat release in the extratropics will be considered in future studies.

According to Fig. 1, one finds some similarities between the distribution of PV and the stream function of the residual circulation particularly in the mid-latitudes. This similarity gives us an impression that PV is somehow conserved during meridional transport. As described in Section 1, however, the residual circulation is generally different from the Lagrangian mean circulation, which is given by a zonal average of Lagrangian motions of air parcels. In this study, we will calculate Lagrangian changes in PV associated with Lagrangian motion of air parcels, in order to investigate the relation between the meridional distribution of PV and the Lagrangian circulations.

The Lagrangian circulation is obtained by trajectory calculations of air parcels which are initially arranged at each grid point of the model at the day 80 of the GCM integration. The numbers of the grid points are 128 in the longitude, 64 in the latitude and 48 in the vertical direction; the total number of air parcels is 393,216. Trajectories of air parcels are calculated by using the 3-h averaged velocity data generated every 3 h from the GCM integration. These data are interpolated with 30-min interval, and positions of the air parcels are obtained by using fourth order Runge-Kutta scheme with a time step of 30 min. Trajectories are calculated for 60 days by using the velocity data from the day 80 to the day 140. We also use different resolutions of the model. The dependency on the resolution is described in Section 6.

3. Results

3.1. *An example of trajectories and Lagrangian changes in PV*

In the first, as an example of the trajectory calculation, meridional and latitude–longitude distributions of air parcels are shown in Fig. 2. Initially, these parcels are equally aligned longitudinally at the latitude 29.3° and the height $\sigma = 0.825$. They consists of 128 parcels. Positions at the days 0, 5, and 10 after the release of the parcels are plotted in these figures. (Hereafter, calculation days are counted from the day when the parcels are released, that is, the day 80 after the GCM integration started.) In addition to the parcel positions, Fig. 2 shows the meridional distributions of zonally averaged potential temperature and PV (Fig. 2a b, c), and PV distribution on an isentropic surface (Fig. 2d, e, f). The value of potential temperature of this surface agrees with the averaged potential temperature possessed by

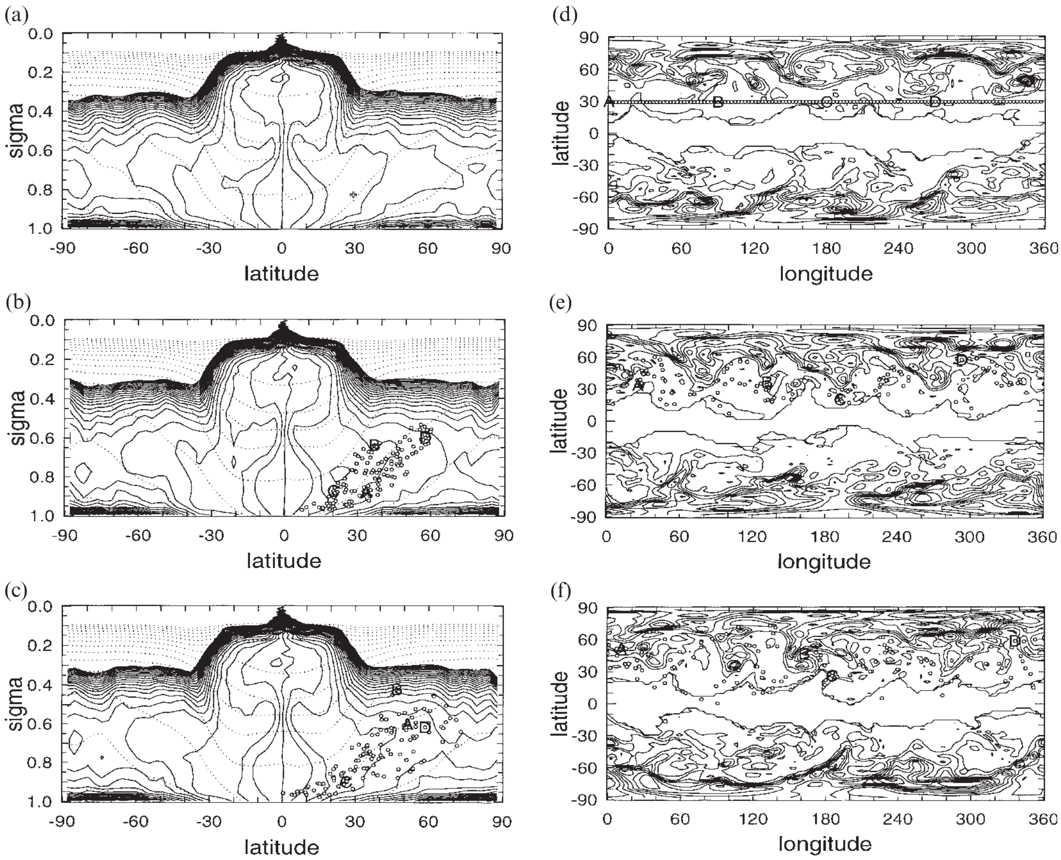

Fig. 2. Positions of the air parcels released from the latitude $\phi = 29.3°$ and the height $\sigma = 0.825$ in the meridional domain for (a) the day 0, (b) the day 5, and (c) the day 10 and in the longitude–latitude domain for (d) the day 0, (e) the day 5, and (f) the day 10. The initial position is indicated by the cross in (a). The parcel positions are indicated by small circles in the other figures. The points indicated by A, B, C and D correspond to the parcel shown by Fig. 3. In (a), (b), and (c), the zonally averaged PV (solid lines) and potential temperature (dotted lines) are added. The contour intervals are the same as in Fig. 1. In (d), (e), and (f), PV values on the isentropic surface that has the averaged value of potential temperature are shown. The contour interval is 0.2 PVU.

the parcels: $\theta = 291.5$ K, initially. Note that each parcel has a different value of potential temperature initially, so that every parcel is not positioned on the same isentropic surface. Fig. 2 shows that, while these parcels disperse along isentropic surfaces, they gradually move to the regions of lower values of potential temperature. The dispersive region of the parcels almost corresponds to the region of wider intervals of the PV contours along the isentropic surfaces. Although almost every parcel stays in the region between 0.2–0.4 PVU (PVU $= 10^{-6}$ kg K m^{-4} s^{-1}), some parcels go into the equatorial lower layers, and some parcels come close to the tropopause transition layers. The filamentary structure of the parcels which is given initially barely remains until the day 5 (Fig. 2e), After that, they are dispersed along the isentropic surfaces.

Among the parcels shown in Fig. 2, we concentrate on the trajectories of the four parcels which have an equal longitudinal interval at the initial time. The 4 parcels are labelled with A, B, C, and D in Fig. 2. The trajectories in the meridional domain and in the horizontal domain are depicted in Fig. 3. From this, we can see that A, B, and D move poleward, whereas C moves equatorward initially. As shown by Fig. 2f, B is caught up into a vortex of high-PV region, which is located at around longitude 60° initially (Fig. 2d), 120° at the day 5 (Fig. 2e), and 160° at the day 10 (Fig. 2f). As the vortex moves eastward, B moves north-eastward, and cyclonically goes round the vortex. This kind of cyclonic motion of the trajectory is also seen in the later period of the trajectory of A and in the middle period of the trajectory of D.

Values of physical quantities possessed by the air parcels can be taken from the output data from the GCM calculation. By interpolating the grid data of potential temperature and PV at the positions of the parcels, we obtain the values of potential temperature and PV of each parcel. Changes of potential temperature and PV thus obtained corresponds to the respective Lagrangian changes. These quantities should be conservative under adiabatic and non-frictional conditions. In the present situation, however, they are not conserved since diabatic heating/cooling, friction and numerical diffusion exist. Fig. 4 shows time sequences of potential temperature and PV for the four parcels shown in Fig. 3. The thick lines in Fig. 4 show the averaged values over all the 128 parcels shown in Fig. 2 and the two dashed lines in each figure show the averaged value plus and minus the root mean square of the deviation from the averaged value at respective time. Fig. 4a indicates that A, B, and D clearly have a decreasing tendency of potential temperature, while C does not have an appreciable tendency. The averaged value of potential temperature is 291.5K at the day 0, and slightly decreases to 291.3 K at the day 10. On the other hand, Fig. 4b indicates that the averaged value of PV has an increasing tendency, though the PV values of each parcel are very variable. PV of B increases as the parcel B is caught up in the high-PV vortex; its value becomes larger than 0.4 PVU at the day 9. PV of D also increases around the day 5; this increase corresponds to the poleward movement of the parcel around a cyclonic vortex.

3.2. Meridional distributions of Lagrangian mean change

The same analysis as shown in Fig. 4a, b is applied to all the grid points on the meridional plane. The zonal averaged Lagrangian changes in potential temperature and PV for 10 days are shown in Fig. 5a, b, respectively. In these figures, values are shown at each meridional grid point of the initial positions. Changes in potential temperature in Fig. 5a represent diabatic effect. They are basically cooled in the middle layers of the troposphere except for the equatorial heating zone and and heating layers in the lower levels in the low- and mid-latitudes. There are also large heating and cooling regions in the stratosphere $\sigma < 0.2$, but we do not pay any attention to the stratosphere.

In Fig. 5b, changes in PV have a rather complicated distribution. It can be thought that this distribution is significant if there are corresponding patterns in the other hemisphere with opposite signs. Characteristic patterns are as follows. (In the following, signs of PV or PV change are for the northern hemisphere). In the equatorward latitudes from 40°, PV is increasing except for the region of the subtropic jets (around $\phi = 30°$ and $\sigma = 0.4$) where PV is decreasing. In the poleward latitudes from 40°, PV is decreasing except for the polar lower layers where PV is increasing. In the stratosphere, PV tendency is positive in the equatorward latitudes from 30° whereas it is nega-

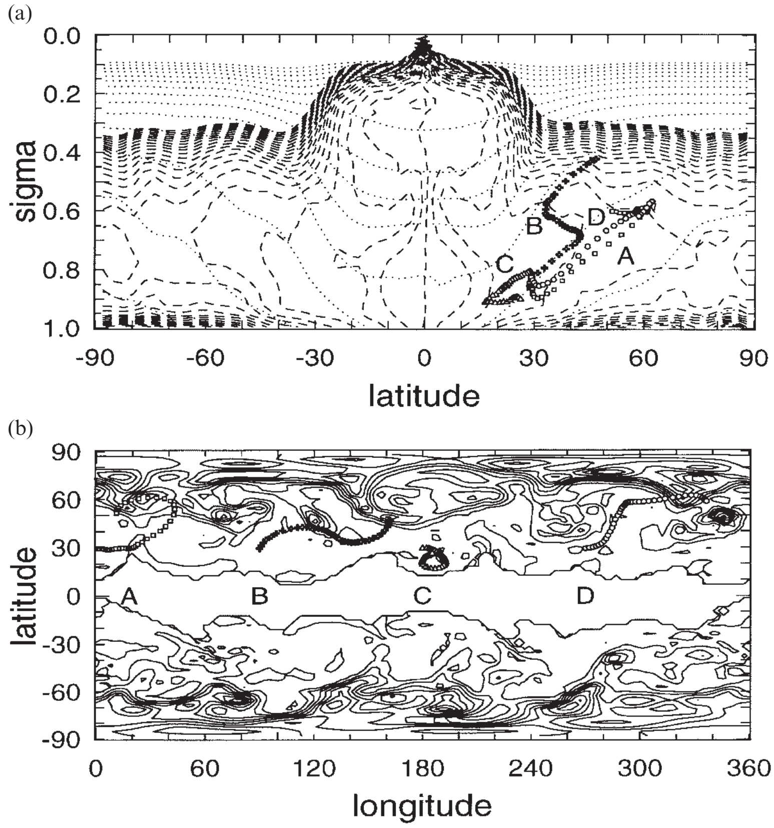

Fig. 3. The parcel trajectories for 10 days in (a) the meridional domain and (b) the longitude–latitude domain. Four parcels are released from the latitude $\phi = 29.3°$ and the height $\sigma = 0.825$. The initial longitudes are 0°, 90°, 180°, and 270° for the parcels A, B, C, and D, respectively. The positions of every 6 h are marked. As in Fig. 2a, b, the zonally averaged PV and potential temperature at the day 0 are added in (a), and the PV distribution on the isentropic surface at the day 0 is added in (b).

tive in the poleward latitudes. There is a quadrupole patten in the middle layers of the equatorial region.

To see what effects determine the PV changes shown in Fig. 5b, we calculate source terms of PV. In the framework of the hydrostatic approximation, the PV tendency equation is given as follows (Hoskins, 1991):

$$\frac{\mathrm{d}P}{\mathrm{d}t} = P\frac{\partial(\theta Q/T)}{\partial\theta} - g\frac{\partial\theta}{\partial p}\boldsymbol{k}\cdot\nabla_{\mathrm{H}}\times\boldsymbol{F}_{\mathrm{H}}, \tag{7}$$

where P is PV, θ is potential temperature, Q is diabatic heating, $\boldsymbol{F}_{\mathrm{H}}$ is horizontal components of frictional forcing, and $\boldsymbol{k}\cdot\nabla_{\mathrm{H}}\times$ is the vertical component of the rotation operator. The first term on the right hand side is PV change due to diabatic effect, and the second term is PV change due to frictional effect. In the case that the small scale diffusion in the free atmosphere is negligible, Q and $\boldsymbol{F}_{\mathrm{H}}$ are given by the diabatic heating eq. (1), and the Rayleigh friction eq. (6), respectively. The distribution of Q is similar to Fig. 5a: Q is positive in the equatorial region and the boundary layers and it is negative in the middle layers of the troposphere. The first term on the right hand side of eq. (7) is approximately proportional to the vertical gradient of heating rate multiplied by the Coriolis parameter f. In general, therefore, this term is negative in the lower troposphere and positive in the upper troposphere. Fig. 6a shows the zonally averaged distribution of 10 days integral of this diabatic term along each trajectory. The

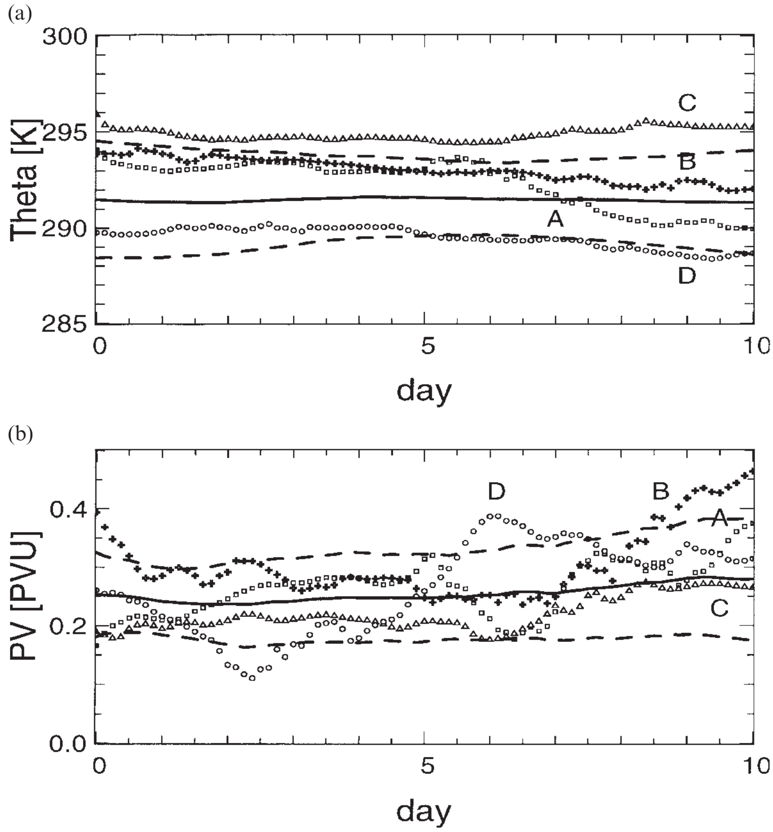

Fig. 4. Time sequences of the Lagrangian changes in (a) potential temperature and (b) PV for the four parcels shown in Fig. 3. The thick solid lines show the averaged values and the dashed lines show the averaged value plus and minus the root mean square (RMS) of the deviation from the averaged values. The 4 marked time sequences are those of the labelled parcels in Fig. 2 and in Fig. 3.

contribution of the diabatic term is larger as in the lower levels; the tendency is negative in the northern hemisphere. Note that there is a quadrupole structure near the equator as seen in Fig. 5b. On the other hand, $\boldsymbol{F}_{\mathrm{H}}$ given by eq. (6) is non-zero only below the levels $\sigma_{\mathrm{B}} = 0.8$. The 2nd term on the right-hand side of eq. (7) is mainly determined by the zonal winds component near the surface; for instance, it has a positive tendency in the region where the surface westerlies increase in the poleward direction. (In the zonal average, this term is positive near the latitude 30° which is the boundary of the Hadley and the Ferrel cells. It is also positive in the polar regions, if there is westerly in the polar surface.) The 10 days integral of this frictional term along each trajectory is shown in Fig. 6b. This shows that it has a positive tendency in the most regions in the lower troposphere from the latitude 30° to the pole. Regions of negative tendency can be seen in the lowest levels of the Hadley cells and the latitude around 60°.

All the change in PV shown in Fig. 5b cannot be attributable to the diabatic effect or the frictional effect shown in Fig. 6a, b, respectively. As described in Section 2, a horizontal diffusion on the σ surfaces is introduced to the numerical model in the vorticity, divergence and temperature fields. It might be thought that this effect corresponds to the effect of the stirring and mixing by the smaller scale flows which are not resolved in the model. The horizontal diffusion, however, is originally introduced by the requirement of numerical stability, and does not mean a physical parameterisation of the small scale turbulence of

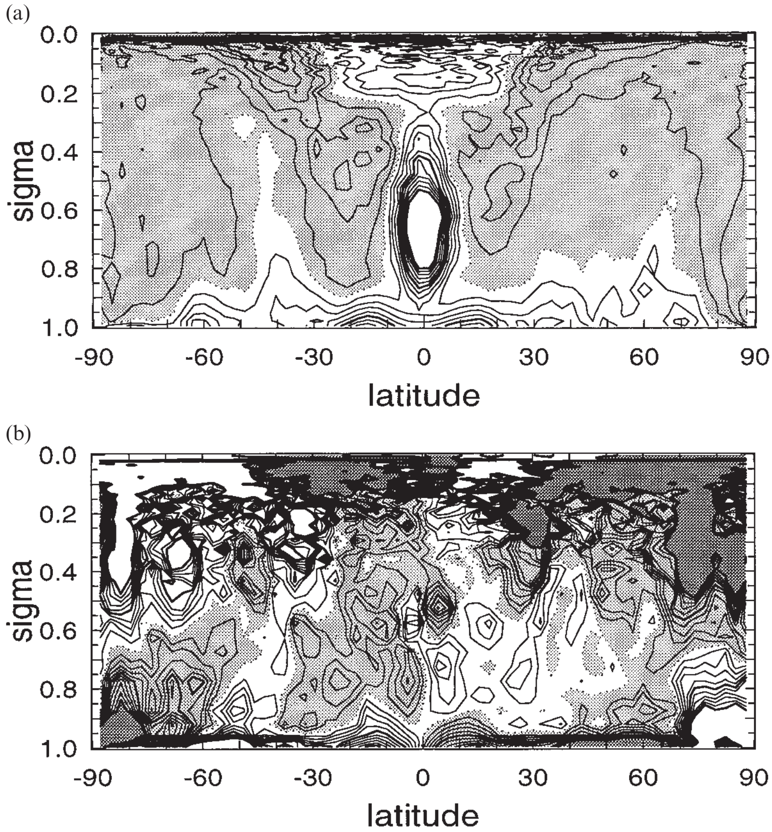

Fig. 5. Meridional distributions of the Lagrangian mean changes in (a) potential temperature and (b) PV during 10 days. The contour interval is 1 K (10 days)$^{-1}$ for (a) and 0.02 PVU (10 days)$^{-1}$ for (b). The dotted line is zero and the gray scale means negative values. As for (b), only the contours in the range from -0.2 PVU (10 days)$^{-1}$ to $+0.2$ PVU (10 days)$^{-1}$ are shown.

the real flows. For instance, a problem might occur in such a region where isentropic surfaces have a large inclination against σ surfaces, since the diffusion of temperature along σ surfaces may bring about an artificial diabatic heating or cooling. This will happen near the subtopic jets, for instance. Further more, numerical discretisation will introduce the following effects. First, the model used in this study is governed by the primitive equations in which vorticity, divergence and temperature are prognostic variables. This implies that the numerical scheme does not guarantee conservation of PV along air parcels in each time step. Second, calculation of PV also introduces a truncation error which comes from the vertical derivative of potential temperature (see Section 5). Therefore, it is possible that PV is not conserved along Lagrangian trajectories even if there are no diabatic and frictional effects or numerical diffusion. The problems listed above are inherent in the use of the spectrum model in the σ-coordinates. A better estimation of PV change in the numerical model may depend on development of the other types of numerical models such as the contour advection model in which PV is used as a prognostic variable (e.g. Dritschel and Ambaum, 1997). However, the approach like this study may be valuable since there have been many studies on PV evolution by using the spectrum model. In order to see how much the numerical truncation may affect the results, we have tested dependencies of the reso-

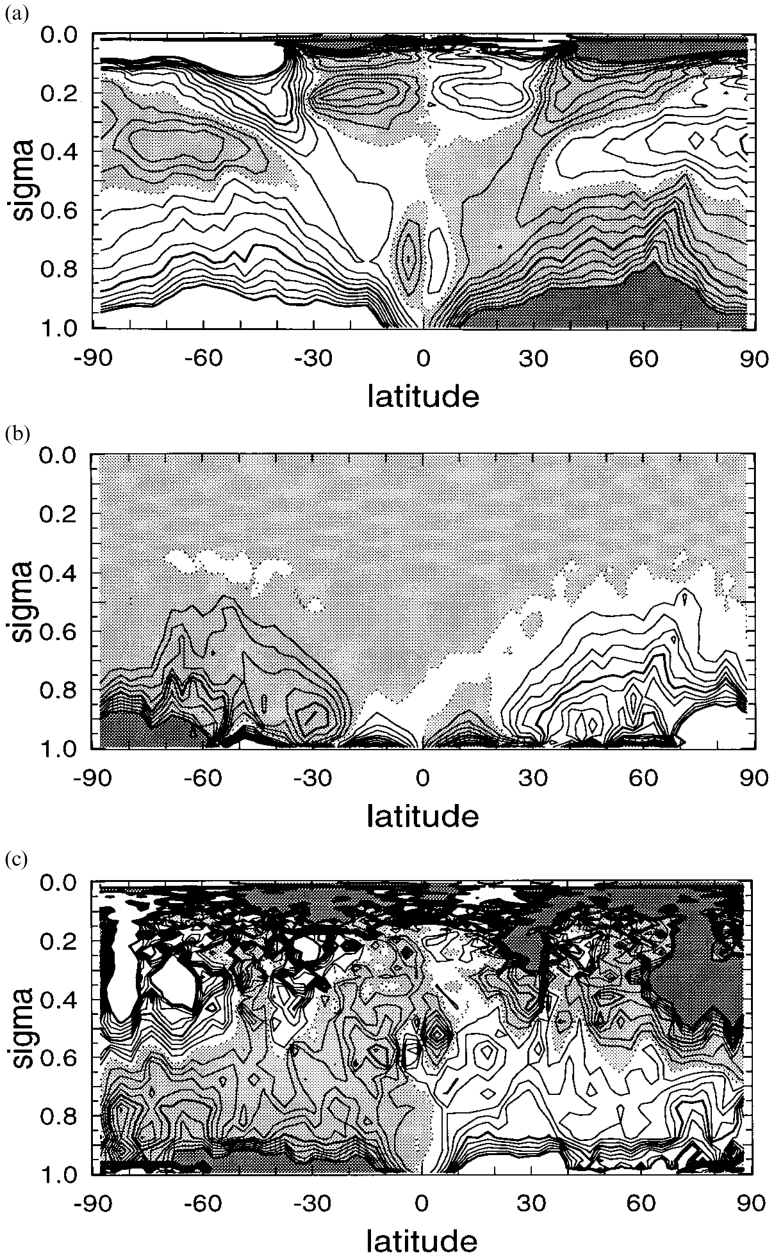

Fig. 6. Meridional distributions of the source term of PV due to (a) diabatic effect, (b) frictional effect and (c) "mixing effect" (see text). As in Fig. 5b, the contour interval is 0.02 PVU (10 days)$^{-1}$.

lution of the numerical model on the PV fields and PV changes by changing vertical and horizontal resolutions (Section 6).

The Lagrangian change in PV calculated in the model may be written as

$$\frac{\mathrm{D}P}{\mathrm{D}t} = P\,\frac{\partial(\theta Q/T)}{\partial\theta} - g\,\frac{\partial\theta}{\partial p}\,\boldsymbol{k}\cdot\nabla_{\mathrm{H}}\times\boldsymbol{F}_{\mathrm{H}} + D, \qquad (8)$$

in which velocity fields used in the Lagrangian time derivative on the left-hand side has a relatively larger scale resolved in the model. The PV change shown in Fig. 4b corresponds to the integral on the left-hand side along each trajectory. On the other hand, D may be interpreted as an effect of small scale mixing which is not resolved in the model, although this interpretation should be reserved since many numerical effects described above contaminates this term. The effect of this term will be referred to "mixing effect" in short. Fig. 6c shows the meridional distribution of the mixing effect which is given by the subtraction of Fig. 6a, b from Fig. 5b. In comparison to Fig. 5b, the negative tendency of PV in the lower layers disappear and the large positive tendency in the polar lower regions is greatly reduced. As a result, Fig. 6c shows basically positive tendency in the lower half of the troposphere, and negative tendency in the upper half of the troposphere. These tendencies are thought to reflect the effect of the mixing on isentropic surfaces. Since air parcels spread along isentropic surfaces as shown in Fig. 2, parcels which have smaller PV in the lower layers will be mixed with those parcels which have larger PV in the upper layers, and vice versa.

As in Fig. 5b for the Lagrangian mean change in PV during 10 days, Fig. 7 shows changes for further longer durations (20, 30, 40, 50, and 60 days). Note that values are converted to the change for 10 days; the same unit as in Fig. 5b. As the integral time becomes longer, the smaller scale structure seen in Fig. 5b becomes smoothed out. The distribution of the PV change during

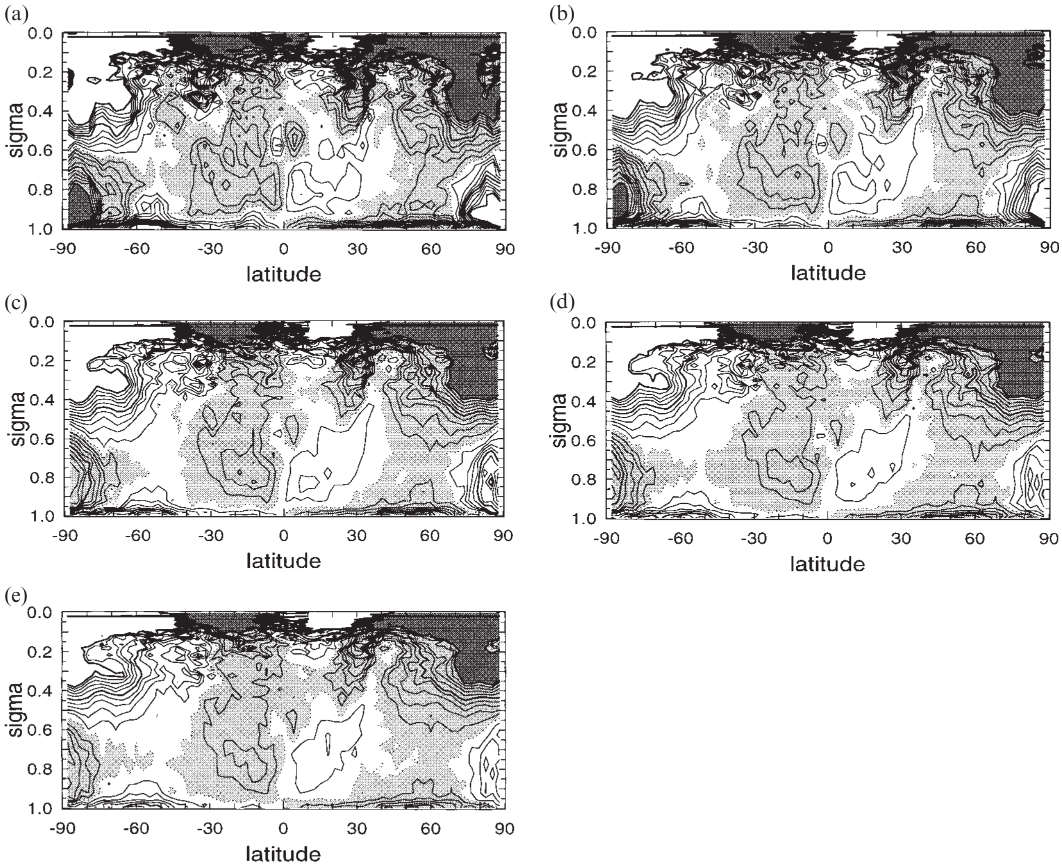

Fig. 7. As in Fig. 5b but for the Lagrangian mean changes in PV during (a) 20, (b) 30, (c) 40, (d) 50, and (e) 60 days. The contour interval is 0.02 PVU (10 days)$^{-1}$.

60 days has a different pattern between the "Underworld" and the "Middleworld": the "Underworld" is defined to be the region below the isentrope that starts from the equatorial surface and reach the tropopause at the pole, whereas the "Middleworld" is the region above the Underworld in the troposphere (Hoskins, 1991). In the Middleworld, if compared in a same isentrope, the PV change is positive in the lower and equatorward region and negative in the upper and poleward region. The isentropes in the Middleworld are further divided into two parts: one is those which reach the subtropical jets (the upper part of the Middleworld) and the other is those which reach the tropopause in the mid- and high-latitudes (the lower part of the Middleworld; see Fig. 1). The boundary of the positive and the negative tendency regions of PV is different between the two parts of the Middleworld. In the upper part, the negative region persists for 60 days near the subtropic jets, whereas the positive region also remains around 20°. In the lower part of the Middleworld, the boundary of the positive and negative tendency regions is located around the 40°. As for the Underworld, the positive tendency region in the equatorward latitudes vanishes on the entire isentropes, except for the positive region exists persistently in the polar lower layers due to the frictional effect (Fig. 6b). The negative tendency of PV in the Underworld reflects the heating near the surface boundary and the equatorial flow along the the surface.

3.3. *Lagrangian changes of characteristic parcels*

Let us examine characteristic points shown in Figs. 5b and 7. We choose the following three points: P: ($\phi = 29.3°$, $\sigma = 0.825$), Q: ($\phi = 49.2°$, $\sigma = 0.477$), R: ($\phi = 29.3°$, $\sigma = 0.477$). The evolution of the parcels released from P is already shown in Figs. 2–4. Fig. 8 shows every meridional position of the parcels at the day 10 released from P, Q, and R. In each figure, the initial position is indicated by the cross, and the mean position at the day 10 is by the square. The Lagrangian mean trajectory passes the two positions. In Fig. 8, those parcels which experienced larger change in PV than the root mean square of changes are designated by circles (positive) and triangles (negative). In general, positive PV changes are seen in the parcels which moved poleward, and negative PV changes are seen in the parcels which moved equatorward. Some exceptions are seen particularly for the parcels released from Q: two parcels shown by triangles poleward from 80° (Fig. 8b) must have larger PV in the initial state. Fig. 8c shows the parcels released in the region of the subtropical jets. In this case, the parcels are also spreading along the isentropic surfaces even in the subtropics. Some parcels moved equatorward are put into the tongue region of PV near the equator.

As shown by Fig. 5b, the 10 days change in the Lagrangian mean of PV is positive at P, and is negative at Q and R. The signs of the Lagrangian mean changes in PV correspond to whether the Lagrangian mean trajectory crosses the PV contours downgradient or upgradient. The Lagrangian mean trajectory of P is poleward along the isentrope and it is also upgradient of the PV contours in the relatively homogenised region of PV. The Lagrangian mean trajectory of Q crosses the PV contours downgradient and equatorward, while the mean values of potential temperature slightly decreases. Though there is some meandering in the Lagrangian mean trajectory of Q, it is not meaningful since each parcel has a large amplitude of motion. The trajectory of R also crosses the PV contours downgradient.

3.4. *Relation between Lagrangian mean motions and PV distribution*

Figs. 9a, b show meridional distributions of the Lagrangian mean trajectories for 10 days and 60 days, respectively. The initial points of the air parcels are indicated by small black circles in Fig. 9a and by open circles in Fig. 9b. In these figures, only the trajectories for every four grid points in the vertical and every two grid points in the latitude are shown. In Fig. 9a, the contours of potential temperature are added by dotted lines and those of PV by solid lines. This shows relations between the PV contours and the Lagrangian mean motion. We can see nearly parallel relationship between the isentropes and the Lagrangian mean motions. In particular, in the lower level ($\sigma = 0.875$) from 20° to 45°, the Lagrangian mean motions is poleward, whereas in the upper level ($\sigma = 0.477$) around 50°, it is equatorward. Although these trajectories are almost parallel to the contours of potential temperature, their directions are opposite. These trajectories reflect large

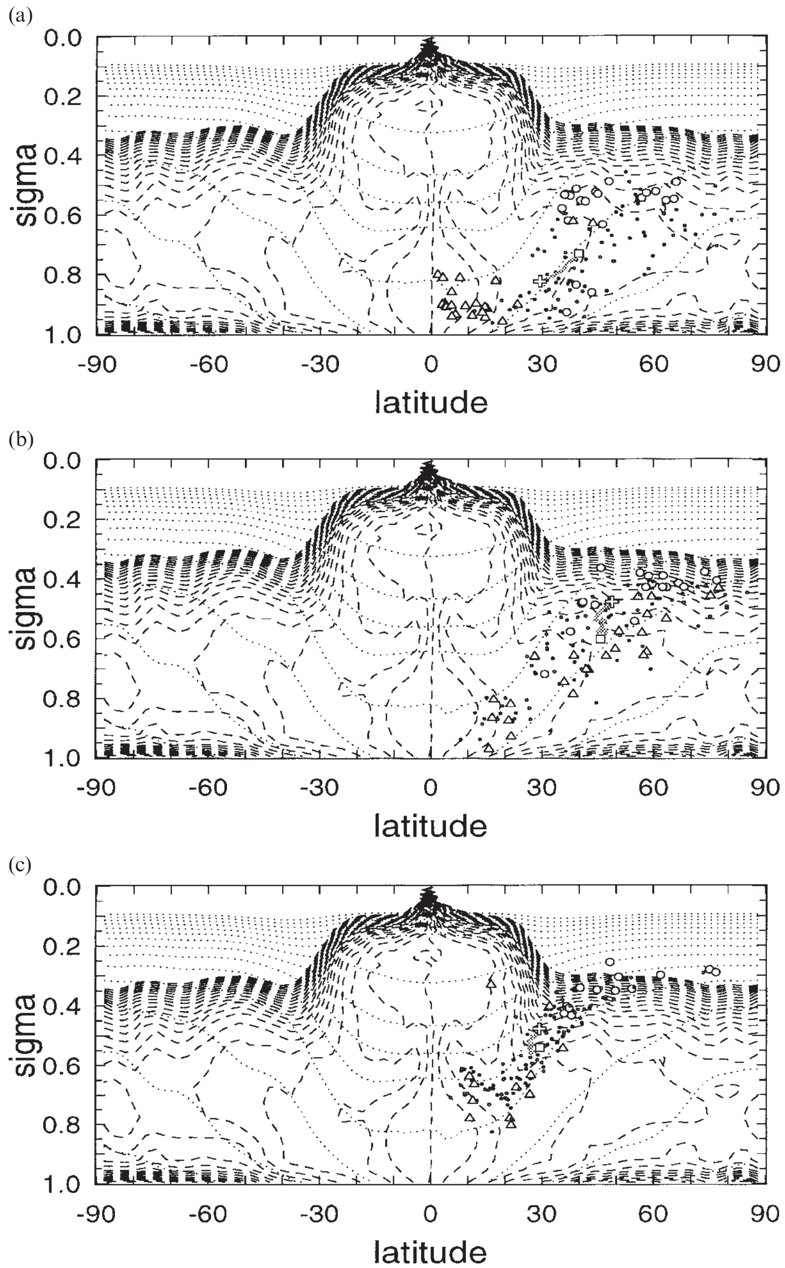

Fig. 8. Positions of the air parcels at the day 10 and the Lagrangian mean trajectory for 10 days (thick line). Open circle means PV change is greater than the root mean square (RMS) change in PV, white triangle means PV change is smaller than RMS, and the other parcels are shown by small black points. The initial position is indicated by plus and the mean position at the day 10 is by open square. (a) is for the same parcels as in Fig. 2, which are released from $\phi = 29.3°$ and $\sigma = 0.825$, (b) is for the parcels from $\phi = 49.2°$ and $\sigma = 0.477$, and (c) is for the parcels from $\phi = 29.3°$ and $\sigma = 0.477$. As in Fig. 2, the zonally averaged PV and potential temperature at the day 0 are added.

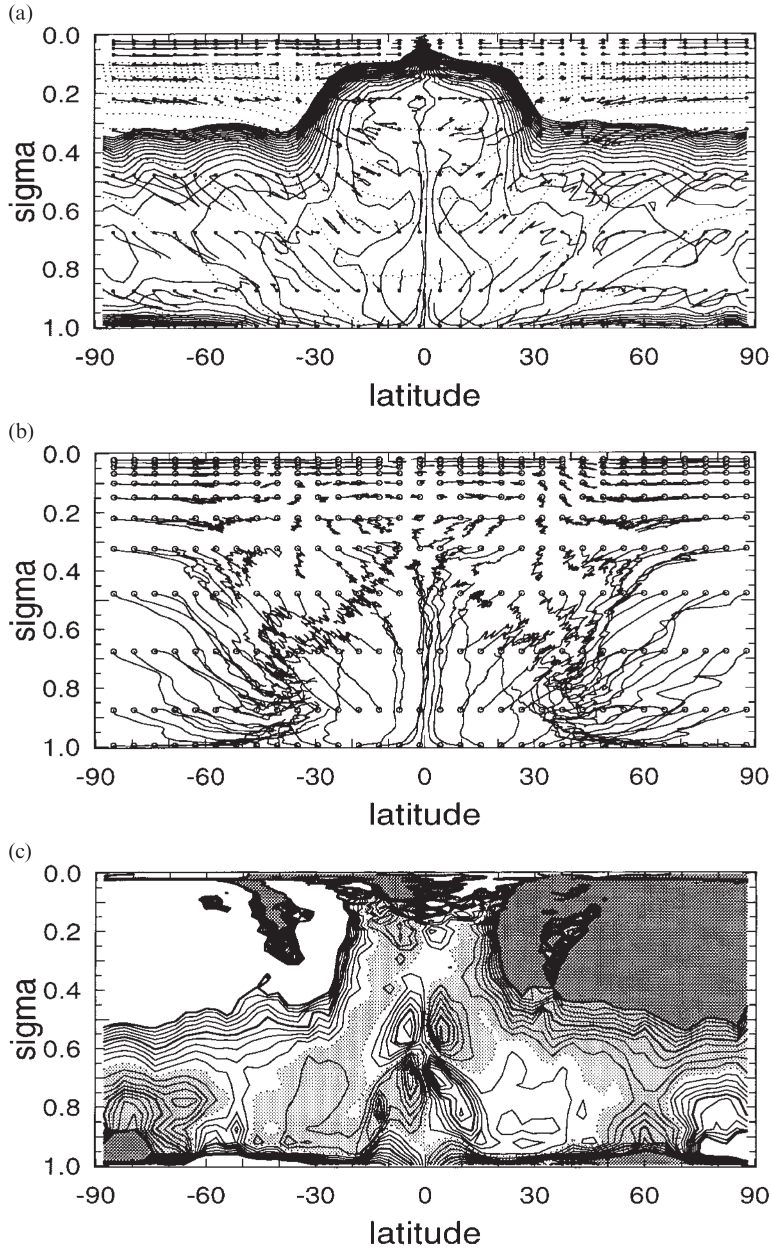

Fig. 9. The Lagrangian mean trajectories for (a) 10 and (b) 60 days. (c) is the meridional distribution of changes in zonal mean PV corresponding to the Lagrangian mean displacements during 10 days (see text). Trajectories for every four vertical and every two meridional grid points are shown. In (a), the initial positions are indicated by small black points. As in Fig. 2, contours of the zonally averaged PV and potential temperature are added. In (b), The initial positions are indicated by open circles. Contour interval for (c) is the same as in Fig. 5b.

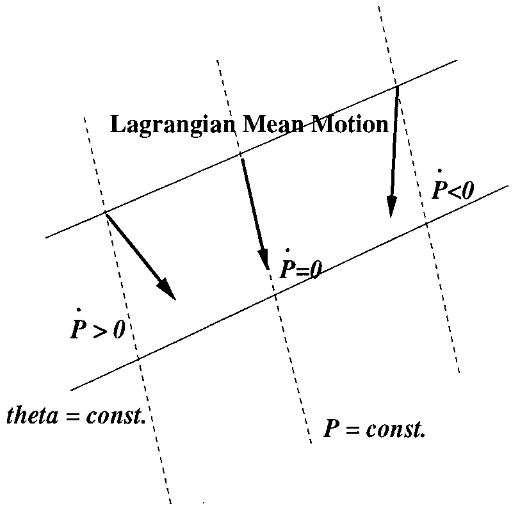

Fig. 10. Schematic relation between the contours of PV, potential temperature and the Lagrangian mean motions.

amplitude motions on isentropic surfaces, as described in Fig. 8. The Lagrangian mean motions are convergent in these regions in the sense that their directions are toward the centre of the motions (Noda, 1988). In the upper level in the subtropics ($\phi=20°$, $\sigma=0.477$), the Lagrangian mean motions are downward. Although this corresponds to the downward motion of the Hadley circulation, they are slightly equatorward than the PV contours as a result of the relatively larger equatorward spreading along isentropic surfaces. In the lower level ($\sigma=0.875$) of the poleward latitudes from 45°, the equatorward motion becomes predominant. This region is in the Underworld in which the Lagrangian mean motions reflect the equatorward flow near the lower surface.

Fig. 9c shows the meridional distribution of the changes in zonal mean values of PV at the Lagrangian mean positions of the parcels at the interval of 10 days. The change at each meridional grid point is defined by a difference between the zonal mean value of PV at the Lagrangian mean position at the day 10 and the initial value of zonal mean PV. For instance, for the parcels released from the points on the contour of value of zero (the dotted contour), the Lagrangian mean position stays on the same contour of zonal mean PV as that of initial zonal mean PV. The distribution in Fig. 9c resembles that of Figs. 5b or 7. As already indicated in Fig. 8, the Lagrangian mean changes in PV are close to the changes in zonal mean values of PV at the Lagrangian mean positions of the parcels. In particular, the shape of the dotted contour in Fig. 9c resembles a contour of the meridional distribution of PV in the subtropics. This implies that, at the points on this dotted contour, the directions of the PV contour are close to those of the Lagrangian mean motions. The above argument should be used understandings of the larger scale structure, since there are much quantitative difference in the details of the distributions between Figs. 5b and 9c.

4. Summary and discussion

Although this study is based on the results from the idealistic GCM, this simple framework gives a characteristic relationship between the meridional distribution of PV and the meridional circulations. The contours of PV have somewhat similar structure to the streamfunction of the residual circulation and are also parallel to the vectors of the Lagrangian mean motions. The downward motion of the Lagrangian mean circulations in the subtropics corresponds to the vertical directions of the PV contours, and the relatively parallel displacements to the isentropes in the mid-latitudes correspond to the PV homogenisation along the isentropic surfaces. This similarity, however, does not mean that PV is conserved along the meridional Lagrangian mean flow in the time scale of the meridional circulation: PV of each parcel experiences various changes during the time scale of more than 10 days.

In order to examine the Lagrangian change in PV, trajectories of air parcels have been obtained for several tens of days. The well-known characteristics are confirmed in the Lagrangian motions of air parcels. In the mid-latitudes, periodic motions with large amplitudes along isentropic surfaces can be seen. The characteristic time of the spread of the parcels over the isentropic surface is less than 5 days (Fig. 2). In the low-latitudes, air parcels also spread along isentropic surfaces between the subtropic jet and the equatorial area. In particular, those parcels which reach the lower boundary layer are transported equatorward by the equatorward flow near the surface.

Next, we have examined changes in PV associated with each parcel trajectory. In general, if an air parcel moves poleward, PV increases due to the mixing with the higher PV of environmental airs, and if an air parcel moves equatorward, PV decreases. (The signs of PV and its tendencies are for the northern hemisphere. In the southern hemisphere, these signs are opposite.) In the case that the Lagrangian mean motion is poleward, it implies that there are more numbers of air parcels which move poleward than those which move equatorward, so that the Lagrangian mean change in PV becomes positive. To a first approximation, the Lagrangian mean changes in PV are related to the meridional distributions of PV and the Lagrangian mean motions in the meridional plane. This relation is shown in Fig. 10: if the Lagrangian mean displacement crosses the PV contours upgradient, the mean value of PV increases, and if the displacement crosses the PV contours downgradient, the mean value of PV decreases. In particular, in the extratropics where isentropic surfaces incline toward higher altitudes as latitudes become higher, there are periodic motions with large amplitudes along the isentropic surfaces. In these regions, owing to the mixing with environmental airs, air parcels gain higher PV if they move to the higher latitudes, and their PV is diluted if they move equatorward. In the central region of the periodic motions, changes in PV become small since poleward movements and equatorward movements equally occur. Only in this region, the Lagrangian mean change in PV becomes zero, and directions of the contours of PV become close to the displacement of the Lagrangian mean motions.

For the time scale of more than 10 days, distribution of the Lagrangian mean changes in PV gradually possesses different structure between Underworld and Middleworld. In the Underworld, the meridional circulation is characterised by the isentropic mixing and the equatorward flow near the ground surface. For a longer time scale than 10 days, contributions of the equatorward flow near the ground become large, so that the effects of the sensible heat and the friction in the boundary layers become prominent for the change in PV. On the other hand, in the Middleworld, the mixing effect dominates. If PV tendencies are compared on the same isentrope, PV changes in the equatorial region are positive and PV changes in the polar region or the region near the tropopause are negative. Furthermore, the Middleworld is also divided into two parts: the upper part in which isentropes reach the subtropic jets, and the lower part in which isentropes reach the extratropical tropopause. In each part, the centre of PV mixing is located different latitudes: about 25° vs 45°. In the Middleworld, the shape of the contour of no change in PV resembles a contour of the zonally averaged PV (Fig. 9).

The boundary between the Underworld and the Middleworld does not exactly correspond to the boundary of characteristic distributions of PV change, since changes in potential temperature become appreciable during the time scale for the meridional scale. The lower boundary of the region which characterise the mixing along the isentropes should be located at higher level than the boundary between the Underworld and the Middleworld. For further longer time scale than the hemispheric overturning time, air parcels will make a round circuit of the hemisphere. In this case, the Lagrangian mean displacements will direct toward the mass centre of the hemisphere. The Lagrangian mean PV will trivially become close to the hemispherically averaged value of PV. Such a long term change will not be informative.

It might be asked how the Lagrangian mean change in PV shown in the present study are related to the previous works on PV budget analysis in the meridional plane. Edouard et al. (1997) have shown the PV budget analysis on the isentropic coordinates, and obtained distributions of advection of PV due to rotation fields and divergent fields, separately. The meridional distribution of the divergence advection of PV has a strong negative tendency (in the northern hemisphere) near the tropopause and is balanced by the diabatic term. In the present study, this kind of diabatic effect near the tropopause is also seen in Fig. 6a as a positive contribution to the PV change. In the meridional distribution of the rotational advection of PV of Edouard et al., a dipole pattern is seen near the tropopause in the mid-latitude: this pattern consists of positive tendency of PV in the equator side of the tropopause on the isentropic surface and negative tendency in the polar side. This dipole pattern is interpreted as a result from the cross-tropopause mixing of PV. They have argued that the tendency due to the rotational advection is smaller than that due to the divergent advection. Hoskins (1991) has shown an example of PV budget analysis on the isentropic surfaces higher than 310 K in the Middleworld. The dipole pattern near the tropopause is also shown. However, the values are much larger than those of Edouard et al. (1997). The reason for this discrepancy is not clear, but might be due to the difference of the periods of the used data: only one month data is used in Hoskins (1991). In the present analysis, the effect of the cross-tropopause mixing should be represented in Fig. 6c as the mixing term D. In the region of the subtropical jets, the change in PV shows a large negative tendency. The diabatic effect is smaller than the mixing effect, which is different from Edouard et al. However, since the analyses by Edouard et al. (1997) and Hoskins(1991) is based on the Eulerian framework, the Lagrangian change of the present study is not directly compared with their results.

Limitation of the present results comes from the simplification of the model. There are many factors which might be important but are neglected in this study. Firstly, longitudinally asymmetric structures represented by the monsoon circulation in the tropics contribute to the change in PV (Hoerling, 1992). Secondly, effects of latent heat release in the extratropics are neglected in the present study. There is a region where the diabatic term due to latent heat release are positive in the extratropics. In this region, the residual circulation intersects the contours of the potential temperature upgradient, and the Lagrangian trajectory crosses the isentropes in both ways. Then, this effect will give a complicated mixing in the extratropics. Thirdly, local vertical convection in dry or moist sense is not introduced in this model framework. In the problems of Lagrangian transports of materials, vertical mixing due to this kind of convection are important. In the present study, however, only the changes in PV in synoptic scale is relevant, so that it will be suffice to include the effect of convection in a form of the diabatic effect. In this model, since the Newtonian cooling brings temperature close to the reference profile which has a slightly stable stratification, local convection is thought to be included in the radiation effect. It is not clear, however, whether there are systematic differences of PV changes between the case in which the Newtonian cooling is used and the case in which local convection is introduced as a parameterised form. Further more, other important factors such as the seasonal change and the boundary layer turbulence can be counted as differences from the real atmosphere.

Nevertheless, this kind of approach of using a simplified model will give an insight into the understandings of the meridional distribution of PV. The results shown in this paper are only qualitative and diagnostic. For the understandings of the PV distribution, a theoretical model of baroclinic equilibration is required to clear out the difference between the slopes of the contours of PV and the contours of potential temperature, the gradient of PV along the isentropic surfaces in the mid-latitudes, and the difference from the directions of the Lagrangian mean circulation. As one of possible approaches of using the models, we may evaluate an effect of the Hadley circulation intensity on the mid-latitude statistics by changing external parameters. We may explore how the global distribution of PV and the Lagrangian tendency of PV respond to the Hadley circulation intensity. These statistics could be compared to the theories of baroclinic equilibration which is thought to be relevant to the PV homogenisation in the mid-latitudes.

5. Appendix A

Calculation of potential vorticity

The potential vorticity (PV) in the hydrostatic balance has a following form:

$$P = -g\left[f + \frac{1}{a\cos\phi}\left(\frac{\partial v}{\partial \lambda}\right)_\theta - \frac{1}{a\cos\phi}\left(\frac{\partial(u\cos\phi)}{\partial\phi}\right)_\theta\right]\frac{\partial\theta}{\partial p}, \tag{9}$$

where a is the radius of the earth, g is the acceleration due to gravity, λ is longitude, $f = 2\Omega\sin\phi$ is the Coriolis parameter, and Ω is the rotation velocity of the earth. The derivatives of velocities are taken along isentropic surfaces. In the σ-coordinates, this is written as

$$P=\frac{g}{p_s}\left\{-\left[f+\frac{1}{a\cos\phi}\left(\frac{\partial v}{\partial\lambda}\right)_\sigma - \frac{1}{a\cos\phi}\left(\frac{\partial(u\cos\phi)}{\partial\phi}\right)_\sigma\right]\frac{\partial\theta}{\partial\sigma} + \frac{1}{a\cos\phi}\frac{\partial v}{\partial\sigma}\left(\frac{\partial\theta}{\partial\lambda}\right)_\sigma - \frac{1}{a}\frac{\partial u}{\partial\sigma}\left(\frac{\partial\theta}{\partial\phi}\right)_\sigma\right\}. \quad (10)$$

The calculation of PV in this study is based on this form. In general, contributions of the terms including vertical derivatives of u and v in eq. (10) are very small. The derivatives along σ surfaces are calculated with the spectrum method. The derivations with respect to σ is obtained with linear interpolation from values in the two levels just above and below the level considered. Vertical derivative of a physical quantity A at the level k is given by

$$\left(\frac{\partial A}{\partial\sigma}\right)^k=\frac{A^{k+1}-A^{k-1}}{\sigma^{k+1}-\sigma^{k-1}}. \quad (11)$$

Such a linear method would induce large errors where θ changes drastically in the vertical direction, i.e. close to the lowest level and near the tropopause. In this study, we take relatively many layers in the model to diminish the errors, especially near the lower surface. Furthermore, we mainly concentrate on the zonally averaged fields, irregular profiles of PV are smoothed out by the averaging.

6. Appendix B

Dependency on resolutions of the model

We examine how the resolution of the numerical model affects the calculation of PV changes. The results shown in this paper is based on the model with the horizontal resolution T42 and 48 vertical levels. The vertical levels are placed at $\sigma=0.995$, 0.980, 0.955, 0.920, 0.875, 0.825, 0.775, 0.725, 0.675, 0.625, 0.575, 0.525, 0.477, 0.432, 0.392, 0.356, 0.323, 0.293, 0.265, 0.241, 0.218, 0.198, 0.180, 0.163, 0.148, 0.134, 0.122, 0.110, 0.100, 0.0908, 0.0824, 0.0747, 0.0678, 0.0615, 0.0557, 0.0506, 0.0459, 0.0416, 0.0377, 0.0342, 0.0310, 0.0282, 0.0255, 0.0232, 0.0210, 0.0175, 0.0124, 0.00415. We have tested models of other resolutions: T42 and 32 levels (T42L32) and T63 and 32 levels (T63L32). The vertical levels of the 32 level model are placed at $\sigma=0.995$, 0.980, 0.955, 0.920, 0.875, 0.825, 0.750, 0.650, 0.549, 0.462, 0.394, 0.335, 0.285, 0.243, 0.207, 0.176, 0.150, 0.128, 0.109, 0.0925, 0.0787, 0.0670, 0.0571, 0.0486, 0.0414, 0.0352, 0.0300, 0.0255, 0.0217, 0.0175, 0.0124, 0.0415. These levels are placed with approximately equal height difference between $\sigma=0.5$–0.02: the height difference is about 1273m for the 32 level model, and about 771m for the 48 level model.

By using the models with the three different resolutions, we calculate the Lagrangian change in PV. Trajectories of air parcels are calculated for 10 days by using the velocity fields after the day 80 of the integration from the same initial condition. Fig. 11 shows the zonally averaged PV change along trajectories in the cases of T42L32 and T63L32. These figures correspond to Fig. 5b for T42L48. Although there are differences in the distributions of the PV change, overall pattern of their signs are similar in the three cases. Main differences are derived from the differences in the equilibrium states of PV fields, particularly in the subtropical jets and the boundary layers in the subtropics (not shown here). The gradient of PV around the subtropical jets becomes larger as the vertical and horizontal resolution becomes finer. Hence, the negative tendency of PV near the subtropical jets ($\phi=30°$, $\sigma=0.2$), which commonly appear in Figs. 5b and 11, is largest for T42L48 and smallest for T42L32. In the lower layers of the subtropics, the stratification is larger both for T42L32 and T63L32 than that for T42L48; hence, PV values are also larger for T42L32 and T63L32. The large tendency of PV in this region ($\phi=30°$, $\sigma=0.8$) shown in Fig. 11 comes from the larger stratification below this level. The horizontal resolution does not seem to influence the tendency of PV in this region; the vertical resolution has a greater impact on the stability in the lower layers. On the other hand, the "mixing effect" as shown by Fig. 6c has a very similar structure among the three cases; this has a positive tendency in the lower layers and a negative tendency in the upper layers. As this mixing effect reflects many numerical effects described in Section 3, the fact that the distribution of the mixing effect is not so much influenced by the resolution suggests that our results shown in this paper are rather robust at least qualitatively.

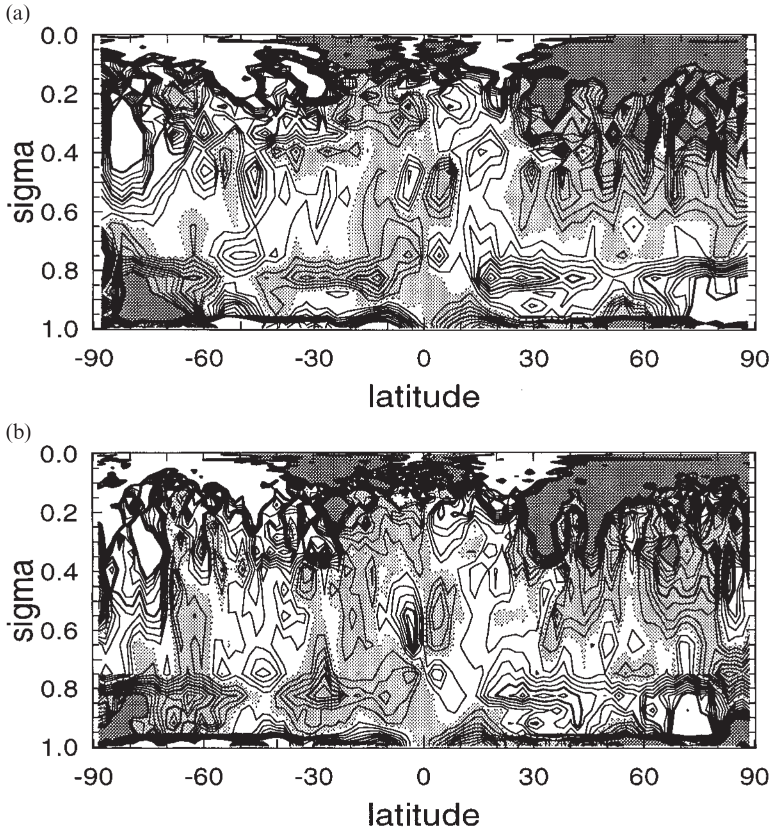

Fig. 11. Dependency of the Lagrangian mean change in PV during 10 days on the resolution of the model: (a) T42L32 and (b) T63L32. Contours intervals are the same as in Fig. 5b.

7. Acknowledgements

The author wishes to thank two anonymous reviewers for valuable comments on the manuscript. This research was supported by Center for Climate System Research, University of Tokyo and National Institute of Environmental Studies (NIES), Japan. A part of this study was carried out while the author was staying at the Centre for Atmospheric Science in the University of Cambridge. This stay was supported by the Japan Society for Promotion of Science and the Royal Society, UK. Centre for Atmospheric Science is supported by the UK Universities Global Atmospheric Modelling Programme, funded by the UK Natural Environmental Research Council.

REFERENCES

Ambaum, M. H. P. 1997. Isentropic formation of the tropopause. *J. Atmos. Sci.* **54**, 555–568.

Andrews, D. G., Holton, J. R. and Leovy, C. B. 1987. *Middle atmosphere dynamics.* Academic Press, Orland, 489 pp.

Andrews, D. G. and McIntyre, M. E. 1978. An exact theory of nonlinear waves on a Lagrangian-mean flow. *J. Fluid Mech.* **89**, 609–646.

Becker, E., Schmitz, G. and Geprags, R. 1997. The feedback of midlatitude waves onto the Hadley cell in a simple general circulation model. *Tellus* **49A**, 182–199.

Brunet, G., Vautard, R., Legras, B. and Edouard, S. 1995. Potential vorticity on isentropic surfaces: climatelogy and diagnostics. *Mon. Wea. Rev.* **123**, 1037–1058.

Dritschel, D. G. and Ambaum, M. H. P. 1997. A contour-advective semi-Lagrangian numerical algorithm for simulating fine-scale conservative dynamical fields. *Q. J. Roy. Meteorol. Soc.* **123**, 1097–1130.

Edmon, H. J., Jr., Hoskins, B. J. and McIntyre, M. E. 1980. Eliassen–Palm cross sections for the troposphere. *J. Atmos. Sci.* **37**, 2600–2612.

Edouard, S., Vautard, R. and Brunet, G. 1997. On the maintenance of potential vorticity in isentropic coordinates. *Q. J. Roy. Meteorol. Soc.* **123**, 2069–2094.

Haynes, P. H. and McIntyre, M. E. 1987. On the evolution of vorticity and potential vorticity in the presence of diabatic heating and frictional or other forces. *J. Atmos. Sci.* **44**, 828–841.

Haynes, P. H. and McIntyre, M. E. 1990. On the conservation and impermeability theorems for potential vorticity. *J. Atmos. Sci.* **47**, 2021–2031.

Held, I. M. and Suarez, M. J. 1994. A proposal for the intercomparison of the dynamical cores of atmospheric general circulation models. *Bull. Amer. Meteorol. Soc.* **75**, 1825–1830.

Hoerling, M. P. 1992. Diabatic sources of potential vorticity in the general circulation. *J. Atmos. Sci.* **49**, 2282–2292.

Holton, J. R. 1992. *An introduction to dynamic meteorology*, 3rd edition. Academic Press, San Diego, 511 pp.

Hoskins, B. J. 1991. Towards a PV-θ view of the general circulation. *Tellus* **43AB**, 27–35.

Hoskins, B. J., McIntyre, M. E. and Robertson, A. W. 1985. On the use and significance of isentropic potential-vorticity maps. *Q. J. Roy. Meteorol. Soc.* **111**, 877–946.

Karoly, D. J., McIntosh, P. C., Berrisford, P., McDougall, T. J. and Hirst, A. C. 1997. Similarities of the Deacon cell in the Southern Ocean and Ferrel cells in the atmosphere. *Q. J. Roy. Meteorol. Soc.* **123**, 519–526.

Kida, H. 1977. A numerical investigation of the atmospheric general circulation and stratospheric-tropospheric mass exchange (I). Long-term integration of a simplified general circulation model. *J. Meteor. Soc. Japan* **55**, 52–70.

Kida, H. 1983. General circulation of air parcels and transport characteristics derived from a hemispherics GCM, Part 2. Very long-term motions of air parcels in the troposphere and stratosphere. *J. Meteor. Soc. Japan* **61**, 510–523.

Johnson, D. R. 1989. The forcing and maintenance of global monsoonal circulations: An isentropic analysis. *Adv. Geophys.* **31**, 43–316.

McIntyre, M. E. and Palmer, T. N. 1984. The "surf zone" in the stratosphere. *J. Atmos. Terr. Phys.* **46**, 825–849.

McIntosh, P. C. and McDougall, T. J. 1996. Isopycnal averaging and the residual mass circulation. *J. Phys. Ocean.* **26**, 1655–1660.

Noda, A. 1988. Generalized Lagrangian-mean (GLM) meridional motions in the troposphere. *J. Meteor. Soc. Japan* **59**, 201–226.

Numaguti, A. 1993. Dynamics and energy balance of the Hadley circulation and the tropical precipitation zones:significance of the distribution of evaporation. *J. Atmos. Sci.* **50**, 1874–1887.

Peixoto, J. P. and Oort, A. H. 1992. *Physics of climate*. American Institute of Physics, New York, 520 pp.

Pierrehumbert, R. T. and Yang, H. 1993. Global chaotic mixing on isentropic surfaces. *J. Atmos. Sci.* **50**, 2462–2480.

Plumb, R. A. 1979. Eddy flux of conserved quantities by small-amplitude waves. *J. Atmos. Sci.* **36**, 1699–1704.

Plumb, R. A. and Mahlman, J. D. 1987. The zonally averaged transport characteristics of the GFDL general circulation/transport model. *J. Atmos. Sci.* **44**, 298–327.

Satoh, M. 1994. Hadley circulations in radiative-convective equilibrium in an axially symmetric atmosphere. *J. Atmos. Sci.* **51**, 1947–1968.

Sun, D.-Z. and Lindzen, R. S. 1994. A PV view of the zonal mean distribution of temperature and wind in the extra-tropical troposphere. *J. Atmos. Sci.* **51**, 751–772.

Townsend, R. D. and Johnson, D. R. 1985. A diagnostic study of the isentropic zonally averaged mass circulation during the first GARP global experiment. *J. Atmos. Sci.* **42**, 1565–1579.